arXiv:1603.06555v2 [cond-mat.mes-hall] 22 Mar 2016

Thermoelectric Transport in Graphene/h-BN/Graphene Heterostructures: A Computational Study

Ransell D'Souza[a], Sugata Mukherjee[a,*]

[a] *S.N. Bose National Centre for Basic Sciences, Block JD, Sector III, Salt Lake, Kolkata 700098, India*

Abstract

We present first principles study of thermoelectric transport properties of sandwiched heterostructure of Graphene (G)/hexagonal Boron Nitride (BN)/G, based on Boltzmann transport theory for band electrons using the bandstructure calculated from the Density Functional Theory (DFT) based plane-wave method. Calculations were carried out for three, four and five BN layers sandwiched between Graphene layers with three different arrangements to obtain the Seebeck coefficient and Power factor in $T \sim 25 - 400$K range. Moreover, using Molecular Dynamics (MD) simulations with very large simulation cell we obtained the thermal conductance (K) of these heterostructures and obtained finally the Figure-of-Merit (ZT). These results are in agreement with recently reported experimental measurements.

Keywords:

PACS: 72.80.Vp, 73.22.Pr, 73.40.-c, 72.20.Pa, 81.05.ue

1. Introduction

The study of thermoelectric transport in nanomaterials has been a topic of intensive research in recent years [1, 2, 3]. Nanomaterials in the form of compound semiconductors, semiconductor multilayers and superstructures offer possibilities to exhibit enhanced thermoelectric Figure-of-Merit (ZT) caused by the simultaneous decrease in thermal conductivity (κ) and increase in electrical conductivity (σ) of the material. This has lead an intensive effort to search for novel materials useful for energy research.

Graphene (G) and Hexagonal boron nitride (h-BN) atomically layered architectures are potential candidates for device applications. 2-D graphene transistors based on lateral heterobarriers have been proposed and investigated from the theoretical point of view [4, 5], which were motivated by the first experimental success in realizing G-BN lateral heterostructures [6]. Based on simulation studies, vertical heter-

obarrier graphene transistors have also been proposed [7], [8]. Britnell et. al. [9] have reported a prototype field-effect tunneling transistor with atomically thin boron nitride acting as a vertical transport barrier. In addition to electron transport, heat dissipation in these graphene based heterojunction devices is found to be dominated by vertical heat transfer [10, 11]. Recently Chen et al [12] have reported thermoelectric transport measurements across G/*h*-BN/G heterostructure with multiple *h*-BN layers. Based on the observed thermoelectric voltage and temperature gradient, they have obtained a Seebeck coefficient (S) of –99.3 μV/K and Thermoelectric Power Factor ($S^2\sigma$) of 1.51×10^{-15} W/K^2 for the heterostructure device, respectively. From the thermal transport measurements of Jo et al [13], thermal conductivity of multilayers of *h*-BN was obtained and finally the Figure-of-merit (ZT) of G/*h*-BN/G heterostructure was estimated [12] to be 1.05×10^{-6}.

Quantum transport in trilayers G/*h*-BN/G and *h*-BN/G/*h*-BN have recently been investigated theoretically by Zhong et al [14], predicting a metal like conduction in low-field regime. Thermoelectric transport in G/*h*-BN nanoribbons have been studied using non-equilibrium Green's function method [15] for different thickness of *h*-BN and Graphene domains. Thermal transport was studied by Kinaci et al [16] in G/*h*-BN nanoribbons using equilibrium molecular dynamics simulation. However, a complete study of thermoelectric transport in G/*h*-BN/G heterostructures with multilayer *h*-BN and comparison to experimental data [12] is apparently not available.

In this paper we report a computational study of the thermoelectric properties of sandwiched heterostructures of Graphene and *h*-BN. We have used density functional theory (DFT) based electronic structure method and Boltzmann transport theory for the band electrons to calculate the electrical conductivity (σ) and Seebeck coefficient (S). A large-scale equilibrium molecular dynamics (MD) simulation using Green-Kubo formalism [17, 18] at constant temperatures was used to compute thermal conductivity (κ) of these heterostructures at various temperatures. Our calculations allow us study of electrical and thermal transport in the directions parallel and normal to the plane of G/*h*-BN/G and thus permits a direct comparison of our simulation results to the experimental data. Our calculations show that for certain configuration of the heterostructured nanomaterials the Power factor and Figure-of-merit (ZT) are close to recent measurements [12]. Moreover, our calculated κ for the multilayers and bulk *h*-BN shows a qualitative agreement with recent experimental results of Jo et al [13]. Calculated κ along orthogonal directions in planar G/*h*-BN striped heterostructures also quantitatively agree with previous calculations [16].

2. Method of Calculation

All the electronic structure calculations were carried out using Density Functional Theory (DFT)

based plane-wave method, as implemented in the Quantum Espresso code [19], using an orthorhombic unit-cell. The generalized gradient approximation (GGA) [20] was used for the exchange-correlation potential and the ultrasoft pseudopotential [21] was used to describe the core electrons. Self-consistent calculations were performed using a converged MonkhorstPack k-point grid [22] of $48 \times 48 \times 2$ with a plane wave basis with kinetic energy cutoff of 40Ry and charge density energy cutoff of 160Ry, respectively. The periodically repeated unit cells are separated by a vacuum spacing of 22Å along the z-direction. This is reasonable since, the widths are typically 10^4 times larger than the height of the sample [13]. We have considered Van der Waals interaction [23, 24] between the layers. For one h-BN layer sandwiched between two graphene layers, we have minimized the total energy and pressure to get a lattice constant of 2.48Å and interlayer distance of 3.21Å. h-BN layers were added at a distance of 3.21Å above the previous layer. It should be noted that addition of layers does not change the pressure of the unit cell. As it has been shown that the AB stacking is the most stable [25] the h-BN layers were fixed to the AB stacking while graphene sheets were changed as shown in fig(1).

2.1. Electrical Conductivity and Thermopower

To calculate the transport properties, we have used the semi-classical Boltzmann transport theory applied to band electrons as implemented by the Boltztrap code [26]. The transport parameters are obtained from the group velocity $v_\alpha(i,\mathbf{k})$ of the band electrons, referring to the i$^{\text{th}}$ energy band and the α $^{\text{th}}$ component of the wavevector $\mathbf{k}$, from the band dispersion $\epsilon(i,\mathbf{k})$ as,

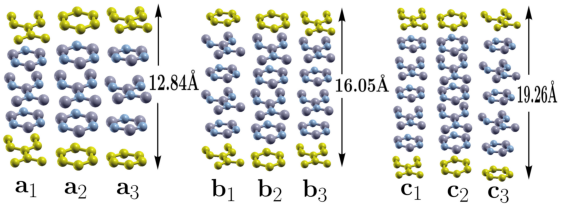

Figure 1: Supercells of G/h-BN/G heterostructures with three (left), four (middle) and five (right) h-BN layers showing three different types of arrangement of Graphene and h-BN layers. The numbers indicate thickness of the heterostructures in Å.

$$v_\alpha(i,\mathbf{k}) = \frac{1}{\hbar}\frac{\partial \varepsilon_{i,k}}{\partial k_\alpha} \tag{1}$$

The electrical conductivity tensor is then written as,

$$\frac{\sigma_{\alpha\beta}(T,\mu)}{\tau} = \frac{1}{V}\int e^2 v_\alpha(i,\mathbf{k})\, v_\beta(i,\mathbf{k})[\frac{-\partial f_\mu(T,\epsilon)}{\partial \epsilon}]d\epsilon \tag{2}$$

Here, f_μ is the Fermi-Dirac distribution function, V is the sample volume and τ is the electron relaxation time, which depends on the electron-electron interaction and e is the electronic charge. Though one would expect that τ would depend on both the band index and $\mathbf{k}$, detailed studies [27, 28] have shown, to a good approximation τ could be independent of direction. Above relation was used to calculate temperature dependent resistivity of two-dimensional CBN nanomaterials recently [29].

The Seebeck coefficient tensor is expressed as,

$$S_{\alpha\beta}(T,\mu) = \frac{1}{eT}\frac{\int v_\alpha(i,\mathbf{k}) v_\beta(i,\mathbf{k})(\epsilon-\mu)[\frac{-\partial f_\mu(T,\epsilon)}{\partial \epsilon}]d\epsilon}{\int v_\alpha(i,\mathbf{k}) v_\beta(i,\mathbf{k})[\frac{-\partial f_\mu(T,\epsilon)}{\partial \epsilon}]d\epsilon} \tag{3}$$

Calculated bandstructure of G/h-BN/G heterostructure [30] indicates that this material is a narrow band gap semiconductor with a band gap $\sim$ 0.05 eV. For the electrical transport

around the energy gap, one can obtain a simpler form of the Seebeck coefficient in Eq. 3, by using the Sommerfeld expansion, to obtain,

$$S = -\frac{\pi^2 k_B^2 T}{3e} \frac{d}{dE} [ln\, \sigma(E)]. \quad (4)$$

Above relation is known as the Mott formula [31], where k_B is the Boltzmann constant. The Power factor is defined as $S^2\sigma$ and the Figure of merit is defined is defined as

$$ZT = \frac{S^2 \sigma T}{\kappa}, \quad (5)$$

where κ is the temperature dependent thermal conductivity.

2.2. Thermal Conductance

In order to obtain the instantaneous heat current ($\mathbf{J}$) as a function of time, one can employ equilibrium molecular dynamics simulations. Moreover, using this heat current, thermal conductivity κ can be evaluated by using the Green-Kubo method [17, 18] or the Einstein relation [32]. Detailed calculations using the latter method have been reported [33, 34, 35, 36, 37]. Here we adopt the Green-Kubo method as implemented in the code LAMMPS [38]. Thermal conductivity is defined as the coefficient that links the macroscopic heat current to the temperature gradient, $\mathbf{J} = -\kappa \bigtriangledown T$. The formula for κ by Green Kubo is given by,

$$\kappa = \frac{1}{3Vk_BT^2} \int_0^\infty \langle \mathbf{J}(0)\mathbf{J}(t)\rangle \mathrm{d}t, \quad (6)$$

where V and T are the volume and temperature. The factor 3 accounts for averaging over the 3 dimensions and the angular brackets refers to the average over time. The macroscopic heat current is given by,

$$\mathbf{J}(t) = \sum_i \mathbf{v}_i e_i + \frac{1}{2} \sum_{i<j} \mathbf{r}_{ij} \big(\mathbf{F}_{ij} \cdot (\mathbf{v}_i + \mathbf{v}_j)\big), \quad (7)$$

where $\mathbf{v}_i$ and e_i are the velocity and site energy of particle i. $\mathbf{F}_{ij}$ is force on the atom i due to its neighbor j from the potential.

Molecular dynamics (MD) simulations were performed first in microcanonical ensemble (NVE) and then the Nosé-Hoover (NVT) ensemble. The constant temperature NVT ensemble requires an additional frictional term [39] to be introduced in Eq 7. To ensure energy conservation of the system, MD simulations were carried out with a time step of 1fs. Five different initial uniform seed velocities were used for the simulations. The value of κ was obtained by averaging over these runs using the standard deviation as the error bar. Preliminary calculations with different number of atoms showed that the standard deviation (error bar) was small when the number of atoms in the simulation cell were around 40000. Therefore, in all MD runs we used simulation cells containing around 40000 atoms. The results of MD simulations are shown in the next section.

We used the Tersoff potential based force field [40], as obtained for *h*-BN by Sevik et al. [34], and for graphene by Lindsay et al. [41]. The Tersoff-parameters for the B-C and N-C bonds were taken from Kinaci et al [16]. To examine this Tersoff-type potential implemented in LAMMPS, we reproduced the results of Kinaci [16] for the thermal conduction in two-dimensional G/*h*-BN stripes by calculating the perpendicular and parallel components of the thermal conductivity in the plane of G/*h*-BN both for the zigzag and armchair interfaces between Graphene and *h*-BN domains. Our calculated value of κ/κ_0, κ_0 being Thermal Conductance of pristine Graphene, compares very well with recent results obtained from non-equilibrium Greens function method [15].

3. Results and Discussions

3.1. Electrical Conductance and Thermopower

The relaxation time for G/*h*-BN/G heterostructures are not known but are typically in the order of 10^{-14}sec. Hence the numerical value used here is 1×10^{-14}sec. Calculations were performed for all topologies as shown in Fig 1 but the results are almost identical except for a small change in Fermi energy (E_F). We therefore report Seebeck coefficient, Power Factor and Figure of Merit for only a specific arrangement as shown in Fig.2 a3,b3,c3. Fig. 2 and 3 refers to the Seebeck coefficient and power factor of G/*h*-BN/G heterostructure having 5 BN layers as shown in Fig.2 c3.

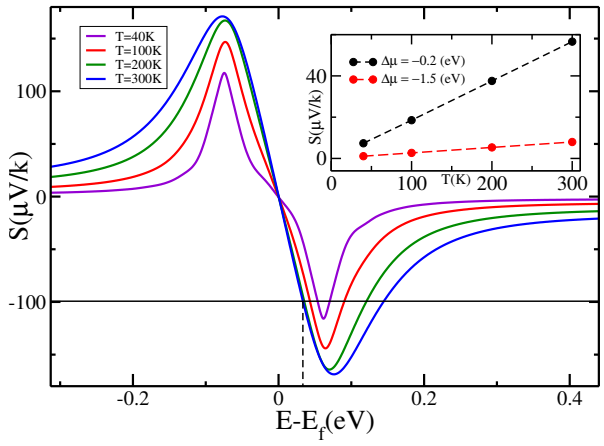

Figure 2: Calculated Seebeck coefficient of G/h-BN/G plotted against energy using the Mott's formula using equation 4 at various temperatures. The black horizontal line refers to the experimental value at T=300K [12]. The inset shows the Seebeck coefficient plotted against Temperature at a constant chemical potential.

Though the band gap of G/h-BN/G heterostructure is formed due to h-BN, the Fermi level does not shift since the number of boron atoms is equal to the number of nitrogen atoms. Further, since boron is an acceptor whereas nitrogen is a donor, the total number of charge carriers n remains the same as that in graphene and hence the conductance at low temperatures, which is essentially proportional to $\sqrt{n}$ is essentially that of graphene [42]. We therefore expect that the form of S, which depends only on conductivity, to have a similar form as that of graphene. In Fig. 2 we see that, as expected, the form of S is that of graphene. However, at very low temperatures the Seebeck coefficient has a flat region around the Fermi energy which is due to the band gap.

In the 40K - 300K temperature (T) range it is seen that the conductivity decreases as T increases. Therefore S increases as T increases as seen in the inset of Fig 2, where we plot S as a function of T at constant chemical potential. The linear dependence of S on T suggests that the mechanism for thermoelectric generation is diffusive thermopower [43]. $S > 0$ for chemical potentials lower than the Fermi energy, $S = 0$ at Fermi energy and $S < 0$ for values greater the Fermi energy. The sign of S indicates the sign of the majority charge carriers. This is also observed experimentally when the gate voltage crosses the charge neutrality point (CNP). $S = 0$ at the CNP. We thus see a direct correspondence between chemical potential and gate voltage. Thus, the gate voltage can tune the chemical potential. As seen in Fig 2, the chemical potential changes sign at the Fermi level. The effect of chemical potential on S can thus be demonstrated by tuning the chemical potential (Fermi energy E_F).

We would like to mention that we have calculated the the components of σ along the cartesian axes, with z-axis being normal to the plane of the G/h-BN/G heterostructure, shown in [30]. Then using the Mott's formula 4 we obtained the Seebeck coefficients along the principal directions [30]. We have obtained a finite S_z near the Fermi energy which contributes to the total Seebeck coefficient which could be due to periodic boundary condition. We feel that the electrical conduction along the z-axis should include contributions also from the other two principal directions, as planar Graphene is used as the contact on both sides of multi-layer h-BN in the experiment [12].

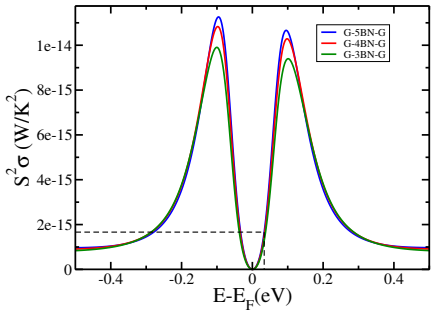

Figure 3: Calculated Powerfactor for different layers in G/h-BN/G. The black horizontal line refers to the powerfactor which corresponds to the chemical potential that yields the experimental Seebeck coefficient by Chen et al [12].

Experimentally the Seebeck coefficient of G/h-BN/G was

measured by applying a temperature gradient between the top and bottom Graphene layers using Raman spectroscopy [12]. For a temperature gradient $\Delta T = 39$ K at a constant thermoelectric voltage $\Delta V = 4$mV, they obtained $S = -99.3\mu$V/K. This method was employed by Chen et al [44] to measure the Seebeck coefficient of G/*h*-BN. To compare our calculations with that of Chen et al [12] we fixed the chemical potential corresponding to the experimentally measured S as shown in Fig. 2. The power factor for the three different arrangements of G/*h*-BN/G heterostructures are shown in Fig. 3. The chemical potential which corresponds to that of the gate voltage of Chen et al [12] has been shown by the black dotted line.

3.2. Thermal Conductance

3.2.1. G/h-BN Planar striped heterostructure

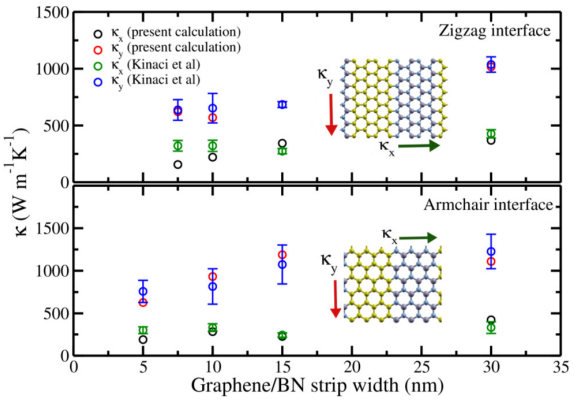

Figure 4: Calculated parallel and perpendicular components of thermal conductivity of *h*-BN/Graphene planar striped heterostructures with zigzag and armchair interfaces between G and *h*-BN domains plotted against the width of the domains. For comparison calculations by Kinaci et al. [16] are also shown. The inset shows the atomic arrangements in each interfaces.

In order to test the equilibrium MD method [38] for the calculation of thermal conductivity, we first calculated κ for two-dimensional striped heterostructures of Graphene and *h*-BN with both armchair and zigzag interfaces between Graphene and *h*-BN domains at $T = 300$K, shown in Fig. 4. The error bars in our calculation are estimated from five different sets of MD runs with different random initial velocities. For comparison we also show the previous calculations by Kinaci et al [16] in the same figure. Our simulation results for κ, both parallel and perpendicular to the crystal edges as shown in the inset, compare quite well with previous calculations [16].

We have also compared the ratio κ/κ_0, κ_0 being thermal conductivity of pristine Graphene, and obtained this to be 0.3203 for the zigzag and 0.3273 for the armchair interfaces, respectively. These results are in excellent agreement with calculations performed using non-equilibrium Green's function method for Graphene and *h*-BN nanoribbons [15]. Therefore, the use of Tersoff potential based force field was found to be satisfactorily applicable for the thermal transport simulations in Graphene and *h*-BN based heterostructures. The calculated κ for G/*h*-BN/G heterostructures for different sample thickness are given in Fig 6 at different T.

3.2.2. Bulk and multilayers of h-BN

In Fig 5 we show the results of thermal conductivity as a function of the temperature (25-400K) calculated from the equilibrium MD simulation at constant temperature (NVT thermostat)for pure *h*-BN 5-, 11-layers and bulk, and compared with the available experimental results of Jo et al [13]. For each calculation, the system was thermalized to the desired temperature first for each set of initial uniform distribution of velocities. κ was calculated for five different sets of initial velocities and the error bar was estimated from the standard deviation.

We found κ increases with T and tend to saturate at $T \sim 220$K for each samples of *h*-BN, with results for 11-layer tending towards the bulk value. Moreover, for each of the three samples of *h*-BN multilayered films, κ shows maxima in the temperature region of 200-250K. We observed an overall agreement of our MD simulation results with recent experimental measurements [13]. For 11-layer and bulk *h*-BN samples the

agreement between the simulation and experimental data is better in temperature range 25-300K, whereas for the 5-layer sample the MD results seem to agree only in the temperature range 100-250K.

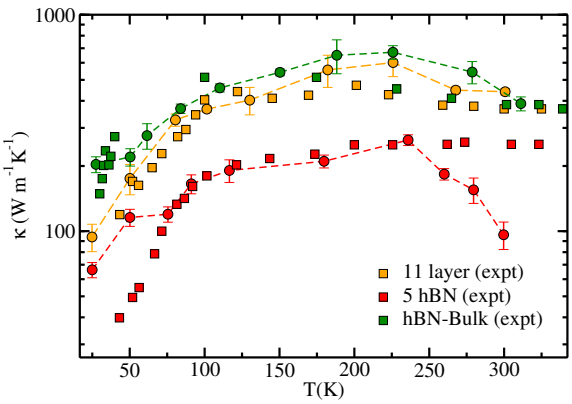

Figure 5: Calculated temperature dependence of the thermal conductivity of h-BN layers of different thickness. Experimental results [13] are shown as squares and present calculations as circles. The error-bars are calculated from five different sets of calculations using different seeds.

Recently, several calculations have been reported on thermal conductivity of single-layer h-BN [45, 46, 47]. Transport calculations by Lindsay et al [45] and Ouyang et al [47], which were calculated from the phonon spectrum using the phonon Boltzmann transport equation, indicate that κ shows a maxima around $T \sim 150$K and decreases with T. Mortazavi et al using MD simulations have reported κ monotonically decreasing with temperature, however all reported values are for temperatures greater than 200K. Our calculated κ for single-layer h-BN shows a monotonic decrease with T, not shown here. The numerical value of κ and its variation with T depends on the direct and Umklapp phonon-phonon scattering mechanism [45] and also on the lifetime of such processes. We plan to investigate these effects using phonon Boltzmann transport theory from the phonon bandstructure later.

3.3. Thermal Conductance, Power Factor and Figure-of-merit of G/h-BN/G Heterostructures

The calculated thermal conductance (K), Power Factor (S^2G) and the Figure-of-merit (ZT) of G/h-BN/G Heterostructures with three-, four- and five-layers of h-BN at the fixed chemical potential has been shown in Fig 6. The chemical potential was fixed to obtain the experimentally observed Seebeck coefficient of -99.3 μV/K as shown in Fig 2. Note, we have plotted the thermal conductance in Fig 6, obtained by multiplying the thermal conductivity (κ) with the height of the G/h-BN/G heterostructure as indicated in Fig 1. Similarly, for the Power Factor (S^2G), we have taken G as the electrical conductance, so that ZT becomes a dimensionless quantity. It can be seen from Fig 3 that as we increase the number of layers, the power factor increases whereas the thermal conductivity decreases with temperature. As a result the power factor increases with temperature. For G/h-BN/G heterostructures having 4- and 5-layers, our calculated values agree well with the experimental results as the temperature tends towards room temperature. From equation 5, the Power factor and Figure of Merit will have the same characteristics when plotted against energy at a given temperature, since κ is a function of only temperature.

We would like to emphasize that our calculations involve electrical transport not strictly along the vertical direction, because the Boltzmann transport theory yields smaller contributions to electrical conductivity along that direction compared to those along x- and y-directions. We have calculated the z-component of the Seebeck coefficient (S_z) [30] and found this to be finite and comparable to S_x and S_y close to the Fermi energy. However, this could be due to the periodic boundary we have implemented also along z- directionwith a vacuum of 22$\mathring{A}$ between the sandwiched layers. The total Seebeck coefficient S shown in Fig 2, however, shows a quantitative agreement with the experimental data [12]. Thus, we conclude that in the thermoelectric measurements [12] the electrical transport may not be strictly along the z-direction as the upper and lower Graphene contacts with multilayer h-BN would allow trans-

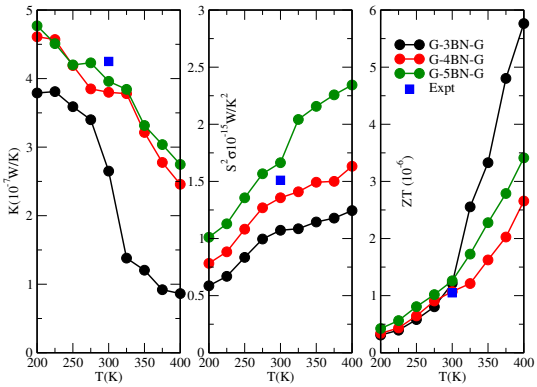

Figure 6: Calculated temperature dependence of Thermal Conductance (K), Power Factor (S^2G) and the Figure-of-merit (ZT) of h-BN layers of different thickness shown in the left, middle and right panels; respectively. The available experimental data [12] in each panel at 300K is also indicated.

port channels involving components along x- and y-directions as well. A good quantitative agreement with experimental data also supports above conclusion.

4. Summary

We have shown that for three, four and five BN layers sandwiched between Graphene layers, the Boltzmann transport theory gives accurate results for the power factor and the Figure-of-merit, comparable to the experimental data. We have also shown that for sufficiently large number of atoms, MD simulations using the Tersoff type potential yields results in good agreement with experiments for thermal conductance of multilayer h-BN, laterally grown striped Graphene and h-BN two-dimensional heterostructures and sandwiched films of Graphene and multilayered h-BN, using the equilibrium Green-Kubo method. Our calculations may be extended to include phonon bandstructure based transport calculations and using non-equilibrium Green's function based methods.

5. Acknowledgment

All computations were performed at the High Performance Parrallel Computer platform at S.N. Bose Centre. One of us R.D. acknowledges support from S.N. Bose Centre through a Senior Research Fellowship. We would like to thank Prof S.D. Mahanti for insightful discussions and valuable comments.

6. References

References

[1] M. Zebarjadi, K. Esfarjani, M. S. Dresselhaus, Z. F. Ren, G. Chen, Perspectives on thermoelectrics: from fundamentals to device applications, Energy Environ. Sci. 5 (2012) 5147.

[2] A. Majumdar, Thermoelectricity in semiconductor nanostructures, Science 303 (2004) 777.

[3] D. G. Cahill, P. V. Braun, G. Chen, D. R. Clarke, S. Fan, K. E. Goodson, P. Keblinski, W. P. King, G. D. Mahan, A. Majumdar, H. J. Maris, S. R. Phillpot, E. Pop, L. Shi, Nanoscale thermal transport. ii. 20032012, Applied Physics Reviews 1 (2014) 011305.

[4] G. Fiori, A. Betti, S. Bruzzone, P. DAmico, G. Iannaccone, Nanodevices in flatland: Two-dimensional graphene-based transistors with high ion/ioff ratio, Proc. Dig. Int. Electron Device Meet 11.4 (2011) 1.

[5] G. Fiori, A. Betti, S. Bruzzone, G. Iannaccone, Lateral graphene hbcn heterostructures as a platform for fully two-dimensional transistors, ACS Nano 6 (2012) 2642.

[6] L. Ci, L. Song, C. Jin, D. Jariwala, D. Wu, A. S. Y. Li, Z. F. Wang, K. Storr, L. Balicasa, F. Liu, P. M. Ajayan, Atomic layers of hybridized boron nitride and graphene domains, Nature Material 9 (2010) 430.

[7] A. Sciambi, M. Pelliccione, M. P. Lilly, S. R. Bank, A. C. Gossard, L. N. Pfeiffer, K. W. West, D. Goldhaber-Gordon, Vertical field effect transistor based on wavefunction extension, Phys. Rev. B 84 (2011) 085301.

[8] W. Mehr, J. C. Scheytt, J. Dabrowski, G. Lippert, Y.-H. Xie, M. C. Lemme, M. Ostling, G. Lupina, Vertical graphene base transistor, IEEE Electron Device Lett. 33 (2012) 691.

[9] L. Britnell, R. V. Gorbachev, R. Jalil, B. D. Belle, F. Schedin, A. Mishchenko, T. Georgiou, M. I. Katsnelson, L. Eaves, S. V. Morozov, N. M. R. Peres, J. Leist, A. K. Geim, K. S. Novoselov, L. A. Ponomarenko, Field-effect tunneling transistor based on vertical graphene heterostructures, Science 335 (2012) 947.

[10] I. Jo, I. K. Hsu, Y. J. Lee, M. M. Sadeghi, S. Kim, S. Cronin, E. Tutuc, S. K. Banerjee, Z. Yao, L. Shi, Low-frequency acoustic phonon temperature distribution in electrically biased graphene, Nano Lett 11 (2011) 85.

[11] E. Pop, V. Varshney, A. K. Roy, Thermal properties of graphene: Fundamentals and applications, MRS Bulletin 37 (2012) 1273.

[12] C.-C. Chen, Z. Li, L. Shi, S. B. Cronin, Thermoelectric transport across graphene/hexagonal boron nitride/graphene heterostructures, Nano Research 8 (2015) 666.

[13] I. Jo, M. T. Pettes, J. Kim, K. Watanabe, T. Taniguchi, Z. Yao, L. Shi, Thermal conductivity and phonon transport in suspended few-layer hexagonal boron nitride, Nano Research 13 (2013) 550.

[14] X. Zhong, R. G. Amorim, R. H. Scheicher, R. Pandey, S. P. Karna, Electronic structure and quantum transport properties of trilayers formed from graphene and boron nitride, Nanoscale 4 (2012) 5490.

[15] K. Yang, Y. Chen, R. D'Agosta, Y. Xie, J. Zhong, A. Rubio, Enhanced thermoelectric properties in hybrid graphene/boron nitride nanoribbons, Phys. Rev. B 86 (2012) 045425.

[16] A. Kinaci, J. B. Haskins, C. Sevik, T. Cagin, Thermal conductivity of bn-c nanostructures, Phys. Rev. B 86 (2012) 115410.

[17] M. S. Green, Markoff random processes and the statistical mechanics of timedependent phenomena. ii. irreversible processes in fluids, J. Chem. Phys 22 (1954) 398.

[18] R. Kubo, Statistical-mechanical theory of irreversible processes. i. general theory and simple applications to magnetic and conduction problems, J. Phys. Soc. Jpn. 12 (1957) 570.

[19] P. Giannozzi, et al., Quantum espresso: a modular and open-source software project for quantum simulations of materials, J. Phys. Condens. Matter 21 (2009) 395502.

[20] J. P. Perdew, K. Burke, M. Ernzerhof, Generalized gradient approximation made simple, Phys. Rev. Lett. 77 (1996) 3865.

[21] D. Vanderbilt, Soft self-consistent pseudopotentials in a generalized eigenvalue formalism, Phys. Rev. B 41 (1990) 7892.

[22] H. J. Monkhorst, J. D. Pack, Special points for brillouin-zone integrations, Phys. Rev. B 13 (1976) 5188.

[23] S. Grimme, J. Antony, S. Ehrlich, S. Krieg, A consistent and accurate ab initio parametrization of density functional dispersion correction (dft-d) for the 94 elements h-pu, J. Chem. Phys. 132 (2010) 154104.

[24] S. Grimme, S. Ehrlich, L. Goerigk, Effect of the damping function in dispersion corrected density functional theory, J. Comp. Chem. 32 (2011) 1456.

[25] T. Kaloni, S. Mukherjee, Comparative study of electronic properties of graphite and hexagonal boron nitride (h-bn) using pseudopotential plane wave method, Modern Physics Letters B 25 (2011) 1855.

[26] G. K. H. Madsen, D. J. Singh, Boltztrap. a code for calculating band-structure dependent quantities, Computer Physics Communication 175 (2006) 67.

[27] W. W. Schulz, P. Allen, N. Trivedi, Hall coefficient of cubic metals, Physical Review B 45 (1992) 10886.

[28] P. Allen, W. Pickett, H. Krakauer, Anisotropic normal-state transport properties predicted and analyzed for high-tc oxide superconductors, Physical Review B 37 (1988) 7482.

[29] R. D'Souza, S. Mukherjee, Electronic structure, phase stability and resistivity of hybrid hexagonal $c_x(bn)_{1x}$ two-dimensional nanomaterial: A first-principles study, Physica E 69 (2015) 138.

[30] The Bandstructure of G-5hBN-G, Calculated conductance (σ) as a function of carrier concentration n, calculated σ_x, σ_y and σ_z as a function of the carrier concentration n, and the calculated components of the Seebeck coefficients as a function of energy are shown in the supplementary information.

[31] M. Cutler, N. F. Mott, Observation of anderson localization in an electron gas, Physical Review 181 (1969) 3.

[32] R. Zwanzig, Time-correlation functions and transport coefficients in statistical mechanics, Annu. Rev. Phys. Chem 16 (1965) 67.

[33] J. Haskins, A. Kinaci, C. Sevik, H. Sevincli, G. Cuniberti, T. Cagin, Control of thermal and electronic transport in defect-engineered graphene nanoribbons, ACS Nano 5 (2011) 3779.

[34] C. Sevik, A. Kinaci, J. B. Haskins, T. Cagin, Characterization of thermal transport in low-dimensional boron nitride nanostructures, Phys. Rev. B 84 (2011) 085409.

[35] C. Sevik, A. Kinaci, J. B. Haskins, T. Cagin, Influence of disorder on thermal transport properties of boron nitride nanostructures, Phys. Rev. B 86 (2012) 075403.

[36] A. Kinaci, J. B. Haskins, T. Cagin, On calculation of thermal conductivity from einstein relation in equilibrium molecular dynamics, J. Chem. Phys. 137 (2012) 014106.

[37] C. Sevik, H. Sevincli, G. Cuniberti, T. Cagin, Phonon engineering in carbon nanotubes by controlling defect concentration, Nano Lett. 11 (2011) 4971.

[38] S. Plimpton, Fast parallel algorithms for short-range molecular dynamics, J Comp Phys 117 (1995) 1–19, we have used the latest release of the code LAMMPS (March 2015 version) in our MD simulations.

[39] S. Berber, Y.-K. Kwon, D. Tománek, Unusually high thermal conductivity of carbon nanotubes, Physical Review Letters 84 (2000) 4613.

[40] J. Tersoff, Modeling solid-state chemistry: Interatomic potentials for multicomponent systems, Phys. Rev. B 39 (1989) 5566.

[41] L. Lindsay, D. A. Broido, Optimized tersoff and brenner empirical potential parameters for lattice dynamics and phonon thermal transport in carbon nanotubes and graphene, Phys. Rev. B 81 (2010) 205441.

[42] K. I. Bolotin, K. J. Sikes, J. Hone, H. L. Stormer, P. Kim, Temperature-dependent transport in suspended graphene, Physical Review Letters 101 (2008) 096802.

[43] V. W. Scarola, G. D. Mahan, Phonon drag effect in single-walled carbon nanotubes, Phys. Rev. B 66 (2002) 205405.

[44] C. C. Chen, Z. Li, L. Shi, S. B. Cronin, Thermal interface conductance across a graphene/hexagonal boron nitride heterojunction, Appl. Phy. Lett. 104 (2014) 081908.

[45] L. Lindsay, D. A. Broido, Enhanced thermal conductivity and isotope effect in single-layer hexagonal boron nitride, Phys. Rev. B 84 (2011) 155421.

[46] B. Mortazavi, L. F. C. Pereira, J.-W. Jiang, T. Rabczuk, Modelling heat conduction in polycrystalline hexagonal boron-nitride films, Scientific Reports 5 (2015) 13228.

[47] T. Ouyang, Y. Chen, Y. Xie, K. Yang, Z. Bao, J. Zhong, Thermal transport in hexagonal boron nitride nanoribbons, Nanotechnology 21 (2010) 245701.